IAC–21–D1.6.1

Coordinated Control of Spacecraft-Manipulator with Singularity Avoidance using Dual Quaternions

Lorenzo Ticozzi
Politecnico di Milano, Italy, lorenzomaria.ticozzi@polimi.it

Giovanni Corinaldesi
D-Orbit SpA, Italy, giovanni.corinaldesi@dorbit.space

Mauro Massari
Politecnico di Milano, Italy, mauro.massari@polimi.it

Francesco Cavenago
Leonardo SpA, Italy, francesco.cavenago@leonardocompany.com

Matthew King-Smith
Georgia Institute of Technology, Georgia (USA), mking-smith@gatech.edu

Panagiotis Tsiotras
Georgia Institute of Technology, Georgia (USA), tsiotras@gatech.edu

The space sector nowadays is characterized by a revived interest from both public and private stakeholders. In the next years, an ever-growing number of satellites will crowd the LEOs and GEOs for commercial, scientific and military purposes; in particular, the development of space-based global Internet coverage will require deployment and maintenance of large satellite constellations. At the same time, space agencies are committed to pushing the boundaries of scientific research and realizing extra-terrestrial outposts which will be the starting point for the future space exploration. Within the context of this development, many challenges are still open. Among them, a key point is the design of systems able to conduct on-orbit servicing (OOS), i.e., inspection, repair, refuelling, upgrade and capture of orbiting targets. These operations are usually carried out with spacecraft-mounted robotic subsystems which must be able to perform autonomously and safely in a complex environment. The modeling and control of these systems is nontrivial, as it involves description of the coupled satellite-manipulator multibody dynamics and a coordinated control strategy to operate the satellite and the robot according to distinct requirements. Building upon previous works, this paper contributes to three aspects of the spacecraft-manipulator problem, namely modeling, control and safety/feasibility of the nominal control solution. Firstly, we model the system in a compact fashion relying on a dual quaternion (DQ) description of the kinematics and dynamics of a multibody system. The DQ formalism expands the well-known unit quaternion algebra, a key tool in the field of spacecraft attitude determination and control, to the analysis of spacecraft-mounted robots. Secondly, we propose a DQ Control Lyapunov Function (DQ-CLF) feedback controller to perform a simultaneous pose-tracking maneuver with both the base and the robot end-effector, where two independent references have to be tracked by the satellite and the robot. Then, we design a novel singularity avoidance method by constraining the nominal solution trajectory using a set of Control Barrier Functions (CBFs). CBFs formally guarantee that the state evolves in a singularity-free subset of the solution space, hence ensuring safety and feasibility of the overall maneuver. As shown by numerical simulations, the proposed approach delivers a great tracking performance, while also keeping the space robot in a nonzero manipulability region.

1. Introduction

The space sector nowadays is characterized by a revived interest from both public and private stakeholders. In the next years, an ever-growing number of satellites will crowd the LEOs and GEOs for commercial,[28] scientific and military purposes; in particular, the development of space-based global Internet coverage will require deployment and maintenance of large satellite constellations. At the same time, space agencies are committed to pushing the boundaries of

scientific research and realizing extra-terrestrial outposts which will be the starting point for the future space exploration.

Within the context of this development, many challenges are still open.[16] Among them, a key point is the design of systems able to conduct on-orbit servicing (OOS), i.e., inspection, repair, refuelling, upgrade and capture of orbiting targets. These operations are usually carried out with spacecraft-mounted robotic subsystems which must be able to perform autonomously and safely in a complex environment. The realization of these systems is inherently complex: whenever the robot and its floating platform are similar-sized, the satellite-base dynamics and kinematics are heavily influenced by the presence of the manipulator, and vice versa. This defines a coupled multibody system, whose elements should, however, be able to operate according to separate requirements; for example, the spacecraft may have to keep a fixed attitude (e.g., to transmit data to the ground or maximize sunlight exposure), while, at the same time, the manipulator may be maneuvering to grasp a non-cooperative target. To achieve this, a coordinated control strategy is needed: the model of the system should be able to reproduce the joint spacecraft-manipulator architecture, while the controller must both compensate the dynamic interactions and exploit them to reach the desired state.

Space robotics literature has dealt with the aforementioned issues in a number of different ways, which can be broadly divided into the free-floating and free-flying categories.[8]

In the first case, the satellite is considered non-actuated, and the uncontrolled motion of the base resulting from the actuation of the manipulator has to be balanced in the manipulator task planning phase. To this aim, Umetani and Yoshida[22] proposed the construction of a Generalized Jacobian Matrix (GJM) to map the desired end-effector velocity into the space of the manipulator joint rates, while also compensating for the motion of the base. The GJM was widely adopted in different formulations of the spacecraft-manipulator control problem.[5,15,30]

An alternative approach to the free-floating case was adopted by Vafa and Dubowsky,[23] who introduced the Virtual Manipulator (VM), a massless kinematic chain equivalent to the free-floating satellite-manipulator, whose origin is attached to the Virtual Ground (VG), a point fixed in the center of mass of the complete system. The VM formulation allows to build a parallel between the floating-base and the fixed-base architectures, hence simplifying the analysis. Liang et al.[12,13] further developed the VM concept by proposing the Dynamically Equivalent Manipulator (DEM), a fixed-base manipulator attached to the ground through a passive spherical joint coincident with the VG. Leveraging this approach, Parlaktuna and Ozan[20] proposed a linear parameterization of the free-floating robot dynamics in order to design an adaptive control method in the joint space. Although appealing from the energy consumption viewpoint, the free-floating type of operations may be unable to fulfil mission goals requiring attitude and/or position control of the base.

Many complexities and limitations encountered within the free-floating scenario can be overcome if the system is considered free-flying, i.e. the satellite-base translation and/or rotation can be controlled. The main drawback of this strategy is the use of resources (fuel, electrical power, etc.) for actuation purposes. Assuming controllability of the spacecraft, previous works addressed the coordinated control of the base and the manipulator. Papadopoulos and Dubowsky[18,19] proposed a control law in the task space using a transposed-Jacobian approach;Oda[17] presented an attitude control system based on the estimate and compensation of the angular momentum induced by the robot arm, exploiting reaction wheels and thrusters as momentum control devices, Jayakody et al.[10] proposed an attitude-only actuated base which is driven towards the desired state thanks to a multi-stage adaptive controller, Antonello et al.[4] modeled the coupled dynamics of the satellite-arm platform using a modified version of the recursive Newton-Euler algorithm.

In this paper the free-flying case is considered, addressing three aspects of the spacecraft-manipulator problem, modeling, control and safety/feasibility of the nominal control solution. Firstly, the system is modeled relying on a dual quaternion (DQ) description of the kinematics and dynamics of a multibody system, which is drawn upon the work of Valverde and Tsiotras.[24] The DQ formalism usefully expands the well-known unit quaternion algebra, a key tool in the field of spacecraft attitude determination and control,[29] to the analysis of spacecraft-mounted robots. Secondly, a DQ Control Lyapunov Function (DQ-CLF) feedback controller is proposed to perform a simultaneous pose-tracking maneuver with both the base and the robot end-effector, where two independent references have to be tracked by the satellite and the robot. Finally, the safety/feasibility of the control is addressed with a novel singularity avoidance

method by constraining the nominal solution trajectory using a Control Barrier Function (CBF), which guarantees that the state evolves in a singularity-free subset of the solution space.

In Section 2 the proposed formulation of the spacecraft-manipulator problem is presented, deriving the DQ form of the kinematic and dynamic relationships, followed by Section 3 where the coordinated controller in the task space is designed using a feedback linearization approach and Section 4 in which the CBF approach to avoid kinematic singularities is shown. Finally, Section 5 presents the results of the numerical simulations.

2. Dual Quaternion Modeling of the System

The dual quaternion formulation is particularly suitable to describe a multibody system with a large number of degrees of freedom, as it is the case for the free-flying manipulator architecture. The reader is referred to the works of Valverde and Tsiotras[24,26] for a thorough discussion on dual quaternions and their properties and for a thorough description of how a multibody system can be modeled using dual quaternions.

2.1 *Dual Quaternions*

The quaternion algebra is defined as $\mathbb{H} \triangleq \{q = q_0 + q_1 i + q_2 j + q_3 k : i^2 = j^2 = k^2 = ijk = -1,\ q_0, q_1, q_2, q_3 \in \mathbb{R}\}$, and a quaternion is written as $q = q_0 + q_1 i + q_2 j + q_3 k$. Quaternions are usually decomposed in a scalar and a vector part, $q = [q_0, \bar{q}]^T$, where $q_0 \in \mathbb{R}$ and $\bar{q} \in \mathbb{R}^3$; this formulation is particularly suitable to represent rigid-body rotations. Since the latter are described by three independent parameters, the unit norm constraint must be respected; hence, unit quaternions expressing rotations are part of the set defined as $\mathbb{H}^u \triangleq \{q \in \mathbb{H} : q^* q = q q^* = 1\}$, $1 = \begin{bmatrix}1, 0_{1\times 3}\end{bmatrix}^T$. The orientation of a frame Y with respect to a frame X is written as the unit quaternion $q_{Y/X}$, and subsequent frame transformations can be obtained through quaternion multiplication, e.g. $q_{Z/X} = q_{Y/X} q_{Z/Y}$.

The quaternion product can be represented as a matrix-vector product by suitably defining the left and right quaternion multiplication operators $[\![\cdot]\!]_L, [\![\cdot]\!]_R : \mathbb{H} \mapsto \mathbb{R}^{4\times 4}$; if $a = \begin{bmatrix}a_0, \bar{a}\end{bmatrix}^T, b = \begin{bmatrix}b_0, \bar{b}\end{bmatrix}^T \in \mathbb{H}$, then $ab \triangleq [\![a]\!]_L * b \triangleq a * [\![b]\!]_R$, with

$$[\![a]\!]_L \triangleq \begin{bmatrix} a_0 & -\bar{a} \\ \bar{a} & a_0 I_3 + [\bar{a}]^\times \end{bmatrix}, \quad [\![b]\!]_R \triangleq \begin{bmatrix} b_0 & -\bar{b} \\ \bar{b} & b_0 I_3 - [\bar{b}]^\times \end{bmatrix}. \quad [1]$$

Given $s \in \mathbb{H}^v$, the operator $[\cdot]^\times : \mathbb{H}^v \mapsto \mathbb{R}^{4\times 4}$ in Eq. (1) has been defined as

$$[s]^\times \triangleq \begin{bmatrix} 0 & 0_{1\times 3} \\ 0_{3\times 1} & [\bar{s}]^\times \end{bmatrix}, \quad [\bar{s}]^\times \triangleq \begin{bmatrix} 0 & -s_3 & s_2 \\ s_3 & 0 & -s_1 \\ -s_2 & s_1 & 0 \end{bmatrix}. \quad [2]$$

Exploiting previous definitions, the dual quaternion set can be defined as $\mathbb{H}_d \triangleq \{\boldsymbol{q} = q_r + \epsilon q_d : \epsilon^2 = 0, \epsilon \neq 0,\ q_r, q_d \in \mathbb{H}\}$, where q_r and q_d are respectively the *real* and *dual* part of the dual quaternion. In the remainder, basic dual quaternion operations follow the definitions given by Valverde and Tsiotras.[25] Analogously to the quaternion case, $\mathbb{H}_d^v \triangleq \{\boldsymbol{q} = q_r + \epsilon q_d : q_r, q_d \in \mathbb{H}^v\}$ is the set of *vector dual quaternions*, while $\mathbb{H}_d^u \triangleq \{\boldsymbol{q} \in \mathbb{H}_d : \boldsymbol{q} \cdot \boldsymbol{q} = \boldsymbol{q}^* \boldsymbol{q} = \boldsymbol{1}\}$ is the set of *unit dual quaternions*. Given $\boldsymbol{s} \in \mathbb{H}_d^v$ and remembering Eq. (2), the operator $[\cdot]^\times : \mathbb{H}_d^v \mapsto \mathbb{R}^{8\times 8}$ can be defined as

$$[\boldsymbol{s}]^x \triangleq \begin{bmatrix} [s_r]^\times & 0_{4\times 4} \\ [s_d]^\times & [s_r]^\times \end{bmatrix}. \quad [3]$$

In order to express dual quaternion multiplication in the more familiar matrix-vector form, recalling Eq. (1), two operators $[\![\cdot]\!]_{\boldsymbol{L}}, [\![\cdot]\!]_{\boldsymbol{R}} : \mathbb{H}_d \mapsto \mathbb{R}^{8\times 8}$ are introduced as follows. If $\boldsymbol{a} = a_r + \epsilon a_d$, $\boldsymbol{b} = b_r + \epsilon b_d$ and $\star$ is the operator representing dual quaternion product as a matrix-vector product, then

$$\boldsymbol{ab} \triangleq [\![a]\!]_{\boldsymbol{L}} \star \boldsymbol{b} \triangleq [\![b]\!]_{\boldsymbol{R}} \star \boldsymbol{a}, \quad [4]$$

where

$$[\![a]\!]_{\boldsymbol{L}} \triangleq \begin{bmatrix} [\![a_r]\!]_L & 0_{4\times 4} \\ [\![a_d]\!]_L & [\![a_r]\!]_L \end{bmatrix}, \quad [\![b]\!]_{\boldsymbol{R}} \triangleq \begin{bmatrix} [\![b_r]\!]_R & 0_{4\times 4} \\ [\![b_d]\!]_R & [\![b_r]\!]_R \end{bmatrix}. \quad [5]$$

2.2 *Rigid Body Motion in Dual Quaternions*

Spatial rigid body motions, which are identified by six independent scalar quantities, can be parameterized using dual quaternions. Since the latter have eight degrees of freedom, two constraints must be enforced, namely $q_r \cdot q_r = 1$ and $q_r \cdot q_d = 0$, with $0 = \begin{bmatrix}0, 0_{1\times 3}\end{bmatrix}^T$. Therefore, dual quaternions parameterizing rigid body motions belong to $\mathbb{H}_d^u$. For

a generic transformation from an X-frame to a Y-frame, $q_r = q_{Y/X}$ and $q_d = \frac{1}{2} q_{Y/X} r^Y_{Y/X}$, where $r^Y_{Y/X} = [0, \bar{r}^Y_{Y/X}]^T$ is the quaternion position of frame Y relative to frame X, expressed in Y. Similarly to subsequent rigid rotations using quaternions, given two pose transformations $\boldsymbol{q}_{Y/X}$ and $\boldsymbol{q}_{Z/Y}$, the change of pose leading from X to Z can be written as $\boldsymbol{q}_{Z/X} = \boldsymbol{q}_{Y/X} \boldsymbol{q}_{Z/Y}$. By defining the *dual velocity*

$$\boldsymbol{\omega}^Y_{Y/X} = \omega^Y_{Y/X} + \epsilon (v^Y_{Y/X} + \omega^Y_{Y/X} \times r^Y_{Y/X}), \quad [6]$$

where $v^Y_{Y/X} = [0, \bar{v}^Y_{Y/X}]^T$ is the linear velocity of frame Y with respect to X, written in Y-frame coordinates, the time evolution of the pose is

$$\dot{\boldsymbol{q}}_{Y/X} = \frac{1}{2} \boldsymbol{q}_{Y/X} \boldsymbol{\omega}^Y_{Y/X} = \frac{1}{2} \boldsymbol{\omega}^X_{Y/X} \boldsymbol{q}_{Y/X}. \quad [7]$$

Note that the same frame transformation can be performed both as $\boldsymbol{\omega}^Y_{Y/X} = \boldsymbol{q}_{Z/Y} \boldsymbol{\omega}^Z_{Y/X} \boldsymbol{q}^*_{Z/Y}$ or as $\boldsymbol{\omega}^Y_{Y/X} = \boldsymbol{q}^*_{Y/Z} \boldsymbol{\omega}^Z_{Y/X} \boldsymbol{q}_{Y/Z}$. To complete this framework, the *dual wrench*, i.e., the force-torque pair applied to any point p in the system, is defined as $\boldsymbol{W}^Y(O_p) = f^Y + \epsilon \tau^Y$, and $f^Y = [0, \bar{f}^Y]^T$, $\tau^Y = [0, \bar{\tau}^Y]^T$, if every quantity is expressed in Y-frame.

2.3 System Configuration and Kinematics

Intuitively, a joint spacecraft-manipulator can be represented as a multibody system made up of a base (the satellite) and one or more structures (the manipulators) attached to the base through some kind of connections. The connections between the manipulators and the base and between the links of the robot are described by different joint types, which define the motion constraint imposed by each connection on its adjacent bodies. Given this framework, the system under analysis can be thought of as a Directed Acyclic Graph $\mathcal{G}(v, e)$,[24] where v is the number of vertices and e the number of edges; the rigid bodies composing the system will be the nodes (vertices), while the joints will act as the edges (Fig. 1). To the aim of this discussion, the joints will be either revolute (R) or prismatic (P), and only one manipulator will be attached to the base, hence originating a one-branch graph. The displacement caused by an R joint will be described by the relative rotation $\theta_{i/\mathfrak{b}_i}$ between the i^{th} joint frame and its parent body frame; similarly, P joints bring about linear displacements specified by $z_{i/\mathfrak{b}_i}$, as reported in Table 1. Some additional quantities must be defined in order to characterize the system in a univocal way: given the overall number of joints J, d_i is the number of degrees of freedom of the i^{th} joint, with $i \in \{1, \dots, J\}$, and $N = J + 1$ is the total number of bodies, according to Fig. 1. $D = \sum_{i=1}^{J} d_i$ is the total number of degrees of freedom allowed by the joints (i.e., the number of degrees of freedom of the manipulator), and conversely $R = \sum_{i=1}^{J} r_i = \sum_{i=1}^{J} (6 - d_i)$ is the number of reaction forces exerted by all the joints. Neglecting joints with $d_i > 1$, the J joint frames are chosen such that the degree of freedom of each joint acts along the local z_i-axis, while the orientation of the other two axes can be chosen arbitrarily. It is common practice to direct one of them towards the subsequent center of mass (see Fig. 2). The link frames $B_{\mathfrak{b}_i}$, $i = \{2, \cdots, N\}$ are fixed at the centers of mass and are oriented as their parent-joint frame ($q_{\mathfrak{b}_{i+1}/i} = 1$), while the satellite frame $B_{\mathfrak{b}_1}$ is aligned with the principal axes of inertia of the base. On the other hand, relative orientations $q_{i/\mathfrak{b}_i}$ between a body and its child-joint frame depend on the joint generalized coordinates, hence being free to vary. If we consider an R joint, $q_{i/\mathfrak{b}_i} = q_{i/\mathfrak{b}_i}(\theta_{i/\mathfrak{b}_i})$. If the system's geometry is known, the distances between the frames are known and, recalling previous considerations, the system can be fully determined from a kinematic viewpoint (Fig. 2).

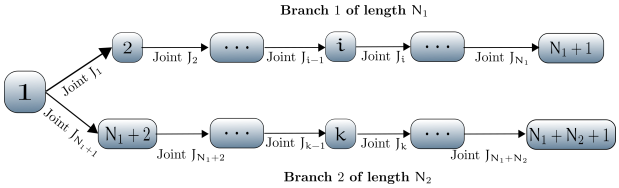

Fig. 1: Graph representation of a spacecraft-mounted manipulator with two branches.

Joint	Γ_{J_i}	$\boldsymbol{d}_i$ (DOF)	L_{J_i}
R	$\theta_{i/\mathfrak{b}_i} \in \mathbb{R}$	1	$[0,0,0,1,0,0,0,0]$
P	$z_{i/\mathfrak{b}_i} \in \mathbb{R}$	1	$[0,0,0,0,0,0,0,1]$

Table 1: Generalized joint coordinates Γ_{J_i} and velocity mapping matrices L_{J_i} for R, P joint types.

The system's forward kinematics can be written as a sequence of pose transformations, as follows:

$$\boldsymbol{q}_{\mathfrak{b}_N/I} = \boldsymbol{q}_{\mathfrak{b}_1/I} \boldsymbol{q}_{1/\mathfrak{b}_1} \left(\prod_{i=2}^{N-1} \boldsymbol{q}_{i/i-1} \right) \boldsymbol{q}_{\mathfrak{b}_N/N-1}. \quad [8]$$

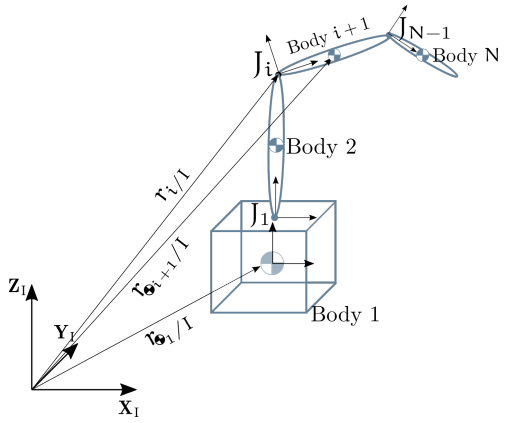

Fig. 2: Definition of frames and distances. The reference frames attached to the centers of mass are not reported for brevity.

From the kinematic chain in Eq. (8) the quaternion position and dual velocity of the end-effector with respect to the inertial frame, $r^{\mathfrak{o}_N}_{\mathfrak{o}_N/I}$ and $\boldsymbol{\omega}^{\mathfrak{o}_N}_{\mathfrak{o}_N/I}$, can be obtained. In particular, recalling that $\boldsymbol{q}_{\mathfrak{o}_N/I} = q_r + \epsilon q_d$, with $q_r = q_{\mathfrak{o}_N/I}$ and $q_d = \frac{1}{2} q_{\mathfrak{o}_N/I} r^{\mathfrak{o}_N}_{\mathfrak{o}_N/I}$, it follows that

$$r^{\mathfrak{o}_N}_{\mathfrak{o}_N/I} = 2 q_r^* q_d. \qquad [9]$$

The detailed derivation of $\boldsymbol{\omega}^{\mathfrak{o}_N}_{\mathfrak{o}_N/I}$ is reported in Valverde and Tsiotras.[25] The vectors $\mathcal{Y}, \Gamma$ are introduced for convenience to collect the dual velocities of all the bodies and the generalized joint coordinates, respectively, as follows

$$\mathcal{Y} \triangleq \left[\left[\boldsymbol{\omega}^{\mathfrak{o}_1}_{\mathfrak{o}_1/I} \right]^T, \cdots, \left[\boldsymbol{\omega}^{\mathfrak{o}_N}_{\mathfrak{o}_N/I} \right]^T \right]^T \in \mathbb{R}^{8N} \qquad [10]$$

and

$$\Gamma \triangleq \left[\Gamma_{J_1}, \cdots, \Gamma_{J_J} \right]^T \in \mathbb{R}^D. \qquad [11]$$

The time evolution of $\mathcal{Y}$ depends on the system's dynamics, while $\dot{\Gamma}$ is constructed by subtracting the velocities of two adjacent bodies expressed in the i^{th} joint frame and selecting the resulting non-null component using the velocity mapping matrices in Table 1,

$$\dot{\Gamma}_{J_i} = L_{J_i} \boldsymbol{\omega}^i_{i/\mathfrak{o}_i} = L_{J_i} \left(\boldsymbol{q}_{\mathfrak{o}_{i+1}/i} \boldsymbol{\omega}^{\mathfrak{o}_{i+1}}_{\mathfrak{o}_{i+1}/I} \boldsymbol{q}^*_{\mathfrak{o}_{i+1}/i} - \right. \\ \left. - \boldsymbol{q}^*_{i/\mathfrak{o}_i} \boldsymbol{\omega}^{\mathfrak{o}_i}_{\mathfrak{o}_i/I} \boldsymbol{q}_{i/\mathfrak{o}_i} \right). \qquad [12]$$

Last, the evolution of the base kinematics can be expressed using Eq. (7)

$$\dot{\boldsymbol{q}}_{\mathfrak{o}_1/I} = \frac{1}{2} \boldsymbol{q}_{\mathfrak{o}_1/I} \boldsymbol{\omega}^{\mathfrak{o}_1}_{\mathfrak{o}_1/I}. \qquad [13]$$

2.4 *System Dynamics*

Following Filipe and Tsiotras,[7] the mass and inertia matrices computed about a rigid body's center of mass can be rearranged into a dual inertia matrix written as

$$M_{\mathfrak{o}_i} \triangleq \begin{bmatrix} 1 & 0_{1\times3} & 0 & 0_{1\times3} \\ 0_{3\times1} & m_{\mathfrak{o}_i} I_3 & 0_{3\times1} & 0_{3\times3} \\ 0 & 0_{1\times3} & 1 & 0_{1\times3} \\ 0_{3\times1} & 0_{3\times3} & 0_{3\times1} & \bar{I}_{\mathfrak{o}_i} \end{bmatrix}, \qquad [14]$$

where $m_{\mathfrak{o}_i}$ is the mass of the i^{th} rigid body, $\bar{I}_{\mathfrak{o}_i} \in \mathbb{R}^{3\times3}$ is the inertia matrix of the same body and I_3 is the 3x3 identity matrix. $M_{\mathfrak{o}_i}$ can be exploited to compute the dual momentum of the i^{th} body about its center of mass, expressed in the local body frame as $\boldsymbol{H}^{\mathfrak{o}_i}_{\mathfrak{o}_i}(O_{\mathfrak{o}_i}) = \boldsymbol{H}^{\mathfrak{o}_i}_{\mathfrak{o}_i/I} \triangleq M_{\mathfrak{o}_i} \star (\boldsymbol{\omega}^{\mathfrak{o}_i}_{\mathfrak{o}_i/I})^{\text{S}}$, where the superscript S denotes the *swap* operator, defined as $\boldsymbol{q}^{\text{S}} = q_d + \epsilon q_r$. Recalling Newton's second principle, $\frac{\mathrm{d}\boldsymbol{H}^{\mathfrak{o}_i}_{\mathfrak{o}_i/I}}{\mathrm{d}t} = \boldsymbol{W}^{\mathfrak{o}_i}_i(O_{\mathfrak{o}_i})$, where $\boldsymbol{W}^{\mathfrak{o}_i}_i(O_{\mathfrak{o}_i}) = f^{\mathfrak{o}_i} + \epsilon \tau^{\mathfrak{o}_i}$ is the net wrench applied on the i^{th} body. Since $\boldsymbol{H}^{\mathfrak{o}_i}_{\mathfrak{o}_i/I}$ is expressed in a rotating body frame, the time derivative of $\boldsymbol{H}^{\mathfrak{o}_i}_{\mathfrak{o}_i}(O_{\mathfrak{o}_i})$ is computed as $\dot{\boldsymbol{H}}^{\mathfrak{o}_i}_{\mathfrak{o}_i/I} + \boldsymbol{\omega}^{\mathfrak{o}_i}_{\mathfrak{o}_i/I} \times \boldsymbol{H}^{\mathfrak{o}_i}_{\mathfrak{o}_i/I} = \boldsymbol{W}^{\mathfrak{o}_i}_i(O_{\mathfrak{o}_i})$. This expression can be expanded, and the following equation is obtained:

$$M_{\mathfrak{o}_i} \star (\dot{\boldsymbol{\omega}}^{\mathfrak{o}_i}_{\mathfrak{o}_i/I})^{\text{S}} + \boldsymbol{\omega}^{\mathfrak{o}_i}_{\mathfrak{o}_i/I} \times \left(M_{\mathfrak{o}_i} \star (\boldsymbol{\omega}^{\mathfrak{o}_i}_{\mathfrak{o}_i/I})^{\text{S}} \right) = \\ = \boldsymbol{W}^{\mathfrak{o}_i}_i(O_{\mathfrak{o}_i}). \qquad [15]$$

After defining a suitable operator $H[\cdot] : \mathbb{R}^{8\times8} \mapsto \mathbb{R}^{8\times8}$ such that $H(M) \star \boldsymbol{a} \triangleq M \star \boldsymbol{a}^S$, and moving the nonlinear velocity term to the right-hand side, Eq. (15) can be rewritten as

$$H(M_{\mathfrak{o}_i}) \dot{\boldsymbol{\omega}}^{\mathfrak{o}_i}_{\mathfrak{o}_i/I} = -\boldsymbol{\omega}^{\mathfrak{o}_i}_{\mathfrak{o}_i/I} \times \left(M_{\mathfrak{o}_i} \star (\boldsymbol{\omega}^{\mathfrak{o}_i}_{\mathfrak{o}_i/I})^{\text{S}} \right) + \\ + \boldsymbol{W}^{\mathfrak{o}_i}_i(O_{\mathfrak{o}_i}). \qquad [16]$$

As illustrated in Fig. 3, the net wrench $\boldsymbol{W}^{\mathfrak{o}_i}_i(O_{\mathfrak{o}_i})$ acting on body i is caused by three different contributions: *body wrenches* $\boldsymbol{W}^{\mathfrak{o}_i}_{\mathfrak{o}_i}(O_{\mathfrak{o}_i})$, which may be due to gravitational disturbances, solar radiation pressure, etc., *actuation wrenches* applied on the adjacent joints $\boldsymbol{W}^j_{\text{act},j}(O_j)$, with $j = \{i-1, i\}$, and *reaction wrenches* $\boldsymbol{W}^i_{\mathfrak{o}_{i+1}/\mathfrak{o}_i}(O_i), \boldsymbol{W}^{i-1}_{\mathfrak{o}_i/\mathfrak{o}_{i-1}}(O_{i-1})$ due to the dynamic interaction between subsequent bodies at their connecting joint. The body wrench on the

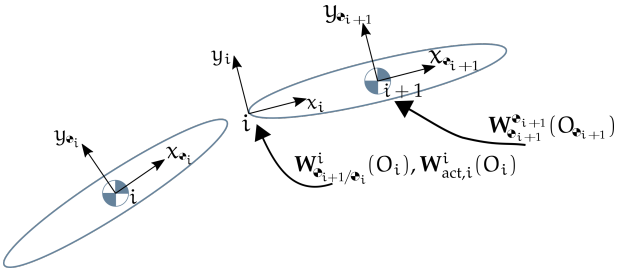

Fig. 3: Wrenches definition and labeling.

base, $\boldsymbol{W}^{\mathfrak{o}_1}_{\mathfrak{o}_1}(O_{\mathfrak{o}_1})$, may include a term describing the control action exerted by the thrusters. As the reaction wrenches are not known *a priori*, a set of R equations expressing the null accelerations of the constrained degrees of freedom of the joints has to be added to Eq. (16). The evolution of the system's dynamics can therefore be written as a system of $8N+R$ equations in the form

$$\begin{bmatrix} \mathcal{S}_{11} & \mathcal{S}_{12} \\ \mathcal{S}_{21} & \mathcal{S}_{22} \end{bmatrix} \begin{bmatrix} \dot{\mathcal{Y}} \\ \mathcal{T} \end{bmatrix} = \begin{bmatrix} \mathcal{B}_1 \\ \mathcal{B}_2 \end{bmatrix}, \qquad [17]$$

where

$$\mathcal{T} \triangleq \left[\left[\tilde{\boldsymbol{W}}^1_{\mathfrak{o}_2/\mathfrak{o}_1}(O_1) \right]^T, \cdots, \left[\tilde{\boldsymbol{W}}^J_{\mathfrak{o}_N/\mathfrak{o}_{N-1}}(O_J) \right]^T \right]^T \in \mathbb{R}^R \qquad [18]$$

gathers the unknown *reduced* * reaction wrenches. $\mathcal{S}_{11} \in \mathbb{R}^{8N\times 8N}$ stores the dual inertia matrices, $\mathcal{S}_{12} \in \mathbb{R}^{8N\times R}$ collects the frame transformations and mapping matrices to couple the reduced reaction wrenches in $\mathcal{T}$ with the rigid body dynamics, $\mathcal{S}_{21} \in \mathbb{R}^{R\times 8N}$ gathers the terms expressing the null accelerations of the constrained degrees of freedom of the joints, and sub-block $\mathcal{S}_{22} \in \mathbb{R}^{R\times R}$ is filled with zeros as no reaction forces appear in the pure kinematic constraint expressed by the second set of equations. On the right hand side, $\mathcal{B}_1 \in \mathbb{R}^{8N}$ stacks the known terms of Eq. (16), as does $\mathcal{B}_2 \in \mathbb{R}^R$ for the reaction wrenches equations. The reader is referred to Valverde and Tsiotras[24] for a step-by-step derivation of the sub-blocks of Eq. (17). Exploiting the structure of Eq. (17), it can be shown[24] that the dynamics of the system can be reduced as follows

$$\begin{aligned} \dot{\mathcal{Y}} &= -\mathcal{S}_{11}^{-1}\mathcal{S}_{12}\mathcal{T} + \mathcal{S}_{11}^{-1}\mathcal{B}_1 \\ &= -\mathcal{S}_{11}^{-1}\mathcal{S}_{12}\left(\mathcal{S}_{21}\mathcal{S}_{11}^{-1}\mathcal{S}_{12}\right)^{-1}\left(\mathcal{S}_{21}\mathcal{S}_{11}^{-1}\mathcal{B}_1 - \mathcal{B}_2\right) + \mathcal{S}_{11}^{-1}\mathcal{B}_1. \end{aligned} \qquad [19]$$

*Recalling that the $\boldsymbol{W}^i_{\mathfrak{o}_{i+1}/\mathfrak{o}_i} \in \mathbb{H}^v_d$, their first and fifth elements are always null and can be neglected; the resulting 6x1 vectors are labeled with a tilde. The same notation will be used in the following of this paper whenever a vector dual quaternion is reduced to a 6x1 vector.

By stacking Eqs. (12), (13) and (19) the system evolution results in a set of $8 + D + 8N$ coupled equations in the form $\dot{x} = f(x,u)$, where $x \triangleq \left[\boldsymbol{q}^T_{\mathfrak{o}_1/I}, \Gamma^T, \mathcal{Y}^T\right]^T$ is the state vector and $u \triangleq \left[\left[\boldsymbol{W}^{\mathfrak{o}_1}_{\mathfrak{o}_1,\text{act}}\right]^T, \left[\boldsymbol{W}^1_{\text{act},1}\right]^T, \cdots, \left[\boldsymbol{W}^J_{\text{act},J}\right]^T\right]^T \in \mathbb{R}^{8(J+1)}$ is the control input, assuming that each joint and the base are actuated.

3. Nonlinear Coordinated Control

In order to achieve coordinated control, starting from the ideas presented in Sections 2.3 and 2.4, we resort to a feedback linearization approach,[11] which will enable tracking of a reference pose and velocity, for both the base and the end-effector.

Once a model of the spacecraft-manipulator in the form $\dot{x} = f(x,u)$ is available, it is necessary to reformulate the equations into a feedback linearizable form,

$$\begin{aligned} \dot{x} &= f(x) + g(x)u, \\ y &= h(x). \end{aligned} \qquad [20]$$

As u exclusively appears in the expression of the accelerations, we need to rearrange the expression of $\dot{\mathcal{Y}}$ in Eq. (19). Hence, we define $\mathcal{B}_1 = \mathcal{B}_{1,\text{act}} + \mathcal{B}_{1,\text{non-act}}$, where $\mathcal{B}_{1,\text{act}}$ can be further rewritten as $\mathcal{B}_{1,\text{act}} = \mathcal{B}_u u$. Eq. (19) becomes then $\dot{\mathcal{Y}} = \Phi(x) + \Psi(x)u$, with $\Phi(x) \in \mathbb{R}^{8N}$ defined as

$$\begin{aligned} \Phi(x) = \mathcal{S}_{11}^{-1}\left(I_{8\times 8} - \mathcal{S}_{12}\left(\mathcal{S}_{21}\mathcal{S}_{11}^{-1}\mathcal{S}_{12}\right)^{-1}\mathcal{S}_{21}\mathcal{S}_{11}^{-1}\right)\mathcal{B}_{1,\text{non-act}} + \\ + \mathcal{S}_{11}^{-1}\mathcal{S}_{12}\left(\mathcal{S}_{21}\mathcal{S}_{11}^{-1}\mathcal{S}_{12}\right)^{-1}\mathcal{B}_2, \end{aligned} \qquad [21]$$

and $\Psi(x) \in \mathbb{R}^{8N\times 8(J+1)}$ corresponding to

$$\Psi(x) = \mathcal{S}_{11}^{-1}\left(I_{8\times 8} - \mathcal{S}_{12}\left(\mathcal{S}_{21}\mathcal{S}_{11}^{-1}\mathcal{S}_{12}\right)^{-1}\mathcal{S}_{21}\mathcal{S}_{11}^{-1}\right)\mathcal{B}_u. \qquad [22]$$

Recalling Eqs. (12) and (13), the overall system dynamics is expressed in a control-affine form as

$$\underbrace{\begin{bmatrix} \dot{\boldsymbol{q}}_{\mathfrak{o}_1/I} \\ \dot{\Gamma}_{J_1} \\ \vdots \\ \dot{\Gamma}_{J_J} \\ \dot{\mathcal{Y}} \end{bmatrix}}_{\dot{x}} = \underbrace{\begin{bmatrix} \frac{1}{2}\boldsymbol{q}_{\mathfrak{o}_1/I}\boldsymbol{\omega}^{\mathfrak{o}_1}_{\mathfrak{o}_1/I} \\ L_{J_1}\boldsymbol{\omega}^1_{1/\mathfrak{o}_1} \\ \vdots \\ L_{J_J}\boldsymbol{\omega}^J_{J/\mathfrak{o}_J} \\ \Phi(x) \end{bmatrix}}_{f(x)} + \underbrace{\begin{bmatrix} 0_{(8+D)\,\times\,8(J+1)} \\ \\ \Psi(x) \end{bmatrix}}_{g(x)} u, \qquad [23]$$

while the output y introduced in Eq. (20) is chosen as $y = \left[\left[\tilde{\boldsymbol{\omega}}^{\mathfrak{o}_1}_{\mathfrak{o}_1/I}\right]^T, \left[\tilde{\boldsymbol{\omega}}^{\mathfrak{o}_N}_{\mathfrak{o}_N/I}\right]^T\right]^T \in \mathbb{R}^{12}$, the collection of the reduced dual velocities of the base and

of the end-effector. Moreover, as the only nonzero entries of vector u are the ones corresponding to the 6 force/torque inputs on the base plus the ones corresponding to the actuated degrees of freedom of the joints [†], the null components of the dual wrenches in u are removed using a suitably assembled mapping matrix $V_{\text{map}} \in \mathbb{R}^{8(J+1) \times 6+D}$; thus, $u = V_{\text{map}}\tilde{u}$, where $\tilde{u} \in \mathbb{R}^{6+D}$ is the reduced control input. The input/output differential relationship[11] needed to feedback linearize the system can be achieved by taking the first-order time derivative of y, which leads to

$$\begin{aligned}\underbrace{\begin{bmatrix}\dot{\boldsymbol{\omega}}^{\mathfrak{o}_1}_{\mathfrak{o}_1/I}\\ \dot{\boldsymbol{\omega}}^{\mathfrak{o}_N}_{\mathfrak{o}_N/I}\end{bmatrix}}_{\dot{y}} &= \underbrace{\begin{bmatrix}\left(\tilde{\Phi}(x)\right)_1\\ \left(\tilde{\Phi}(x)\right)_N\end{bmatrix}}_{D(x)} + \underbrace{\begin{bmatrix}\left(\tilde{\Psi}(x)\right)_1\\ \left(\tilde{\Psi}(x)\right)_N\end{bmatrix} V_{\text{map}}}_{E(x)}\tilde{u} \\ &= D(x) + E(x)\tilde{u}.\end{aligned} \quad [24]$$

In Eq. (24), $\left(\tilde{\Phi}(x)\right)_1, \left(\tilde{\Phi}(x)\right)_N \in \mathbb{R}^6$ and $\left(\tilde{\Psi}(x)\right)_1, \left(\tilde{\Psi}(x)\right)_N \in \mathbb{R}^{6 \times 8(J+1)}$ are extrapolated from $\Phi(x)$ and $\Psi(x)$ by selecting the rows corresponding to the base and end-effector accelerations, while

$$V_{\text{map}} = \begin{bmatrix} V_{\text{act,base}} & 0_{8\times d_1} & \cdots & 0_{8\times d_J} \\ 0_{8\times 6} & V_{\text{act},J_1} & & 0_{8\times d_J} \\ \vdots & & \ddots & \vdots \\ 0_{8\times 6} & \cdots & \cdots & V_{\text{act},J_J} \end{bmatrix}, \quad [25]$$

where $V_{\text{act,base}} \in \mathbb{R}^{8\times 6}$ is the I_8 matrix whose first and fifth columns have been deleted, and the matrices $V_{\text{act},J_i} \in \mathbb{R}^{8\times d_i}$, $i \in \{1, \cdots, J\}$, are obtained with the same procedure, where only the columns corresponding to the actuated degrees of freedom of the i^{th} joint are retained.

3.1 *Spacecraft-Manipulator Control Law*

In order to feedback linearize the system and achieve tracking of a reference velocity, the error variable $e = y - \mathcal{R}$ is defined, where $\mathcal{R} \triangleq \left[\left[\tilde{\boldsymbol{\omega}}^{\mathfrak{o}_1}_{S/I}\right]^T, \left[\tilde{\boldsymbol{\omega}}^{\mathfrak{o}_N}_{E/I}\right]^T\right]^T \in \mathbb{R}^{12}$ includes a known reference velocity for both the base (S subscript) and the end-effector (E subscript). Exploiting the change of variables and recalling that $\dot{\mathcal{R}}$ is known by assumption, the error dynamics $\dot{e} = \dot{y} - \dot{\mathcal{R}}$ is given by

$$\begin{aligned}\dot{e} &= D(x) + E(x)\tilde{u} - \dot{\mathcal{R}} \\ &= \underbrace{D(x) - \dot{\mathcal{R}}}_{\Xi(x)} + E(x)\tilde{u},\end{aligned} \quad [26]$$

where we have defined $\Xi(x) \triangleq D(x) - \dot{\mathcal{R}}$. By choosing

$$\tilde{u} = E(x)^+ \underbrace{(\mu - \Xi(x))}_{b(x)}, \quad [27]$$

with $b(x) \triangleq \mu - \Xi(x)$, then $\dot{e} = \mu$, which means that the error dynamics is linear in the transformed control action μ. Any appropriate choice of μ (e.g., $\mu = Ke$, where K has eigenvalues with strictly negative real part) will drive the system towards a zero error condition. As $E(x) \in \mathbb{R}^{12 \times 6+D}$, $E(x)$ is rectangular whenever $D \neq 6$, i.e. whenever the manipulator is redundant ($D > 6$) or underactuated ($D < 6$). Setting the case $D < 6$ aside, if $D = 6$, then $\tilde{u}$ can be obtained by computing the inverse of $E(x)$, provided that $\text{rank}(E) = 12$. If, instead, matrix $E(x)$ has full rank and $D > 6$, the system has an infinite number of solutions and the Moore-Penrose inverse can be used to select the one with the minimum 2-norm.

After feedback linearizing the system's dynamics, μ must be designed so that the desired velocity and pose tracking requirements are fulfilled. Since the null error condition corresponds to $\boldsymbol{q}_{\mathfrak{o}_1/S}, \boldsymbol{q}_{\mathfrak{o}_N/E} \to \boldsymbol{1}$, $\boldsymbol{\omega}^{\mathfrak{o}_1}_{\mathfrak{o}_1/S}, \boldsymbol{\omega}^{\mathfrak{o}_N}_{\mathfrak{o}_N/E} \to \boldsymbol{0}$, we start by considering a candidate Dual Quaternion Control Lyapunov Function (DQ-CLF) for the equilibrium point $\boldsymbol{q}_{\mathfrak{o}_1/S} = \boldsymbol{1}$, $\boldsymbol{q}_{\mathfrak{o}_N/E} = \boldsymbol{1}$, $\boldsymbol{\omega}^{\mathfrak{o}_1}_{\mathfrak{o}_1/S} = \boldsymbol{0}$, $\boldsymbol{\omega}^{\mathfrak{o}_N}_{\mathfrak{o}_N/E} = \boldsymbol{0}$, defined as

$$\begin{aligned}&V\left(\boldsymbol{q}_{\mathfrak{o}_1/S}, \boldsymbol{\omega}^{\mathfrak{o}_1}_{\mathfrak{o}_1/S}, \boldsymbol{q}_{\mathfrak{o}_N/E}, \boldsymbol{\omega}^{\mathfrak{o}_N}_{\mathfrak{o}_N/E}\right) = \\ &= \frac{1}{2}(\boldsymbol{\omega}^{\mathfrak{o}_1}_{\mathfrak{o}_1/S})^{\text{S}} \circ \left(K_{\mathfrak{o}_1} \star (\boldsymbol{\omega}^{\mathfrak{o}_1}_{\mathfrak{o}_1/S})^{\text{S}}\right) + \\ &\quad + p_{\mathfrak{o}_1}(\boldsymbol{q}_{\mathfrak{o}_1/S} - \boldsymbol{1}) \circ (\boldsymbol{q}_{\mathfrak{o}_1/S} - \boldsymbol{1}) + \\ &+ \frac{1}{2}(\boldsymbol{\omega}^{\mathfrak{o}_N}_{\mathfrak{o}_N/E})^{\text{S}} \circ \left(K_{\mathfrak{o}_N} \star (\boldsymbol{\omega}^{\mathfrak{o}_N}_{\mathfrak{o}_N/E})^{\text{S}}\right) + \\ &\quad + p_{\mathfrak{o}_N}(\boldsymbol{q}_{\mathfrak{o}_N/E} - \boldsymbol{1}) \circ (\boldsymbol{q}_{\mathfrak{o}_N/E} - \boldsymbol{1}),\end{aligned} \quad [28]$$

where $p_{\mathfrak{o}_1}, p_{\mathfrak{o}_N} > 0$ are tunable scalar gains and $K_{\mathfrak{o}_1}, K_{\mathfrak{o}_N} \in \mathbb{R}^{8\times 8}$ are positive-definite diagonal gain matrices. Note that V is a valid DQ-CLF since $V\left(\boldsymbol{q}_{\mathfrak{o}_1/S} = \boldsymbol{1}, \boldsymbol{\omega}^{\mathfrak{o}_1}_{\mathfrak{o}_1/S} = \boldsymbol{0}, \boldsymbol{q}_{\mathfrak{o}_N/E} = \boldsymbol{1}, \boldsymbol{\omega}^{\mathfrak{o}_N}_{\mathfrak{o}_N/E}\boldsymbol{0}\right) = 0$ and $V\left(\boldsymbol{q}_{\mathfrak{o}_1/S}, \boldsymbol{\omega}^{\mathfrak{o}_1}_{\mathfrak{o}_1/S}, \boldsymbol{q}_{\mathfrak{o}_N/E}, \boldsymbol{\omega}^{\mathfrak{o}_N}_{\mathfrak{o}_N/E}\right) > 0$,

[†] Within this work, all the degrees of freedom of the joints are considered actuated. Hence, considering 6 actuation inputs on the base and one for each joint, the reduced actuation vector $\tilde{u}$ has $6 + D$ entries.

$\forall (\boldsymbol{q}_{\mathfrak{o}_1/S}, \boldsymbol{\omega}^{\mathfrak{o}_1}_{\mathfrak{o}_1/S}, \boldsymbol{q}_{\mathfrak{o}_N/E}, \boldsymbol{\omega}^{\mathfrak{o}_N}_{\mathfrak{o}_N/E}) \in \mathbb{H}^u_d \times \mathbb{H}^v_d \times \mathbb{H}^u_d \times \mathbb{H}^v_d \setminus \{\boldsymbol{1}, \boldsymbol{0}, \boldsymbol{1}, \boldsymbol{0}\}$. According to the Lyapunov stability criterion, by dictating a negative value of $\dot{V}$ through an appropriate control action, the system is stabilized at its equilibrium point. In our case, we impose $\dot{V}(x) \leq -W(x)$, with

$$W(x) = k_{\mathfrak{o}_1} (\boldsymbol{\omega}^{\mathfrak{o}_1}_{\mathfrak{o}_1/S})^{\mathrm{S}} \circ (\boldsymbol{\omega}^{\mathfrak{o}_1}_{\mathfrak{o}_1/S})^{\mathrm{S}} + k_{\mathfrak{o}_N} (\boldsymbol{\omega}^{\mathfrak{o}_N}_{\mathfrak{o}_N/E})^{\mathrm{S}} \circ (\boldsymbol{\omega}^{\mathfrak{o}_N}_{\mathfrak{o}_N/E})^{\mathrm{S}}, \quad [29]$$

and $k_{\mathfrak{o}_1}, k_{\mathfrak{o}_N}$ positive scalar gains. Computing the time derivative of the DQ-CLF in Eq. (28) yields

$$\begin{aligned} \dot{V} = (\boldsymbol{\omega}^{\mathfrak{o}_1}_{\mathfrak{o}_1/S})^{\mathrm{S}} \circ \left(K_{\mathfrak{o}_1} \star (\dot{\boldsymbol{\omega}}^{\mathfrak{o}_1}_{\mathfrak{o}_1/S})^{\mathrm{S}} \right) + \\ + 2 p_{\mathfrak{o}_1} (\boldsymbol{q}_{\mathfrak{o}_1/S} - \boldsymbol{1}) \circ \dot{\boldsymbol{q}}_{\mathfrak{o}_1/S} + \\ + (\boldsymbol{\omega}^{\mathfrak{o}_N}_{\mathfrak{o}_N/E})^{\mathrm{S}} \circ \left(K_{\mathfrak{o}_N} \star (\dot{\boldsymbol{\omega}}^{\mathfrak{o}_N}_{\mathfrak{o}_N/E})^{\mathrm{S}} \right) + \\ + 2 p_{\mathfrak{o}_N} (\boldsymbol{q}_{\mathfrak{o}_N/E} - \boldsymbol{1}) \circ \dot{\boldsymbol{q}}_{\mathfrak{o}_N/E}. \end{aligned} \quad [30]$$

Using Eq. (7) to express $\dot{\boldsymbol{q}}_{\mathfrak{o}_1/S}$, $\dot{\boldsymbol{q}}_{\mathfrak{o}_N/E}$, and recalling the swap operator properties [‡], Eq. (30) becomes

$$\begin{aligned} \dot{V} = (\boldsymbol{\omega}^{\mathfrak{o}_1}_{\mathfrak{o}_1/S})^{\mathrm{S}} \circ \left(K_{\mathfrak{o}_1} \star (\dot{\boldsymbol{\omega}}^{\mathfrak{o}_1}_{\mathfrak{o}_1/I} - \dot{\boldsymbol{\omega}}^{\mathfrak{o}_1}_{\mathfrak{o}_S/I})^{\mathrm{S}} + p_{\mathfrak{o}_1} \boldsymbol{q}^*_{\mathfrak{o}_1/S} (\boldsymbol{q}_{\mathfrak{o}_1/S} - \boldsymbol{1})^{\mathrm{S}} \right) + \\ + (\boldsymbol{\omega}^{\mathfrak{o}_N}_{\mathfrak{o}_N/E})^{\mathrm{S}} \circ \left(K_{\mathfrak{o}_N} \star (\dot{\boldsymbol{\omega}}^{\mathfrak{o}_N}_{\mathfrak{o}_N/I} - \dot{\boldsymbol{\omega}}^{\mathfrak{o}_N}_{\mathfrak{o}_E/I})^{\mathrm{S}} + p_{\mathfrak{o}_N} \boldsymbol{q}^*_{\mathfrak{o}_N/E} (\boldsymbol{q}_{\mathfrak{o}_N/E} - \boldsymbol{1})^{\mathrm{S}} \right). \end{aligned} \quad [31]$$

Equating the right hand sides of Eqs. (29) and (31), rearranging the circle products and swapping every term of the equality results in

$$\begin{aligned} \begin{bmatrix} \boldsymbol{\omega}^{\mathfrak{o}_1}_{\mathfrak{o}_1/S} \\ \boldsymbol{\omega}^{\mathfrak{o}_N}_{\mathfrak{o}_N/E} \end{bmatrix} \circ \begin{bmatrix} p_{\mathfrak{o}_1} \left(\boldsymbol{q}^*_{\mathfrak{o}_1/S} (\boldsymbol{q}_{\mathfrak{o}_1/S} - \boldsymbol{1})^{\mathrm{S}} \right)^{\mathrm{S}} + K_{\mathfrak{o}_1} \star (\dot{\boldsymbol{\omega}}^{\mathfrak{o}_1}_{\mathfrak{o}_1/I} - \dot{\boldsymbol{\omega}}^{\mathfrak{o}_1}_{\mathfrak{o}_S/I}) \\ p_{\mathfrak{o}_N} \left(\boldsymbol{q}^*_{\mathfrak{o}_N/E} (\boldsymbol{q}_{\mathfrak{o}_N/E} - \boldsymbol{1})^{\mathrm{S}} \right)^{\mathrm{S}} + K_{\mathfrak{o}_N} \star (\dot{\boldsymbol{\omega}}^{\mathfrak{o}_N}_{\mathfrak{o}_N/I} - \dot{\boldsymbol{\omega}}^{\mathfrak{o}_N}_{\mathfrak{o}_E/I}) \end{bmatrix} = \\ - \begin{bmatrix} \boldsymbol{\omega}^{\mathfrak{o}_1}_{\mathfrak{o}_1/S} \\ \boldsymbol{\omega}^{\mathfrak{o}_N}_{\mathfrak{o}_N/E} \end{bmatrix} \circ \begin{bmatrix} k_{\mathfrak{o}_1} \boldsymbol{\omega}^{\mathfrak{o}_1}_{\mathfrak{o}_1/S} \\ k_{\mathfrak{o}_N} \boldsymbol{\omega}^{\mathfrak{o}_N}_{\mathfrak{o}_N/E} \end{bmatrix}. \end{aligned} \quad [32]$$

Since the term $\left[\left[\boldsymbol{\omega}^{\mathfrak{o}_1}_{\mathfrak{o}_1/S} \right]^T, \left[\boldsymbol{\omega}^{\mathfrak{o}_N}_{\mathfrak{o}_N/E} \right]^T \right]^T$ appears on both sides of the equation, it can be dropped along with the dot products, hence leading to a vector equality

$$\begin{aligned} \begin{bmatrix} p_{\mathfrak{o}_1} \left(\boldsymbol{q}^*_{\mathfrak{o}_1/S} (\boldsymbol{q}_{\mathfrak{o}_1/S} - \boldsymbol{1})^{\mathrm{S}} \right)^{\mathrm{S}} + K_{\mathfrak{o}_1} \star (\dot{\boldsymbol{\omega}}^{\mathfrak{o}_1}_{\mathfrak{o}_1/I} - \dot{\boldsymbol{\omega}}^{\mathfrak{o}_1}_{\mathfrak{o}_S/I}) \\ p_{\mathfrak{o}_N} \left(\boldsymbol{q}^*_{\mathfrak{o}_N/E} (\boldsymbol{q}_{\mathfrak{o}_N/E} - \boldsymbol{1})^{\mathrm{S}} \right)^{\mathrm{S}} + K_{\mathfrak{o}_N} \star (\dot{\boldsymbol{\omega}}^{\mathfrak{o}_N}_{\mathfrak{o}_N/I} - \dot{\boldsymbol{\omega}}^{\mathfrak{o}_N}_{\mathfrak{o}_E/I}) \end{bmatrix} = \\ - \begin{bmatrix} k_{\mathfrak{o}_1} \boldsymbol{\omega}^{\mathfrak{o}_1}_{\mathfrak{o}_1/S} \\ k_{\mathfrak{o}_N} \boldsymbol{\omega}^{\mathfrak{o}_N}_{\mathfrak{o}_N/E} \end{bmatrix}. \end{aligned} \quad [33]$$

Moreover, we define a mapping matrix

$$V_{\mathrm{red}} = \begin{bmatrix} 0 & 1 & 0 & 0 & 0 & 0 & 0 & 0 \\ 0 & 0 & 1 & 0 & 0 & 0 & 0 & 0 \\ 0 & 0 & 0 & 1 & 0 & 0 & 0 & 0 \\ 0 & 0 & 0 & 0 & 0 & 1 & 0 & 0 \\ 0 & 0 & 0 & 0 & 0 & 0 & 1 & 0 \\ 0 & 0 & 0 & 0 & 0 & 0 & 0 & 1 \end{bmatrix} \in \mathbb{R}^{6 \times 8} \quad [34]$$

which can be applied to the dual velocities / accelerations in order to remove their null entries (e.g., $\tilde{\boldsymbol{\omega}}^{\mathfrak{o}_1}_{\mathfrak{o}_1/I} = V_{\mathrm{red}} \boldsymbol{\omega}^{\mathfrak{o}_1}_{\mathfrak{o}_1/I}$) and to the pose terms $\boldsymbol{q}_{\mathfrak{o}_1/S}$, $\boldsymbol{q}_{\mathfrak{o}_N/E}$ to cancel the two dependent equations [§]. Then, we stack V_{red} into a block-diagonal matrix

$$V_{\mathrm{all}} = \begin{bmatrix} V_{\mathrm{red}} & 0_{6\times 8} \\ 0_{6\times 8} & V_{\mathrm{red}} \end{bmatrix} \in \mathbb{R}^{12 \times 16}. \quad [35]$$

After pre-multiplying both sides of Eq. (33) by V_{all}, recalling the definition of the error e and the feedback linearization result $\dot{e} = \mu$, we can write the acceleration terms on the left-hand side of Eq. (33) as follows

$$\begin{aligned} V_{\mathrm{all}} \begin{bmatrix} K_{\mathfrak{o}_1} \star (\dot{\boldsymbol{\omega}}^{\mathfrak{o}_1}_{\mathfrak{o}_1/I} - \dot{\boldsymbol{\omega}}^{\mathfrak{o}_1}_{\mathfrak{o}_S/I}) \\ K_{\mathfrak{o}_N} \star (\dot{\boldsymbol{\omega}}^{\mathfrak{o}_N}_{\mathfrak{o}_N/I} - \dot{\boldsymbol{\omega}}^{\mathfrak{o}_N}_{\mathfrak{o}_E/I}) \end{bmatrix} = \\ \begin{bmatrix} \tilde{K}_{\mathfrak{o}_1} & 0_{6\times 6} \\ 0_{6\times 6} & \tilde{K}_{\mathfrak{o}_N} \end{bmatrix} \begin{bmatrix} V_{\mathrm{red}} (\dot{\boldsymbol{\omega}}^{\mathfrak{o}_1}_{\mathfrak{o}_1/I} - \dot{\boldsymbol{\omega}}^{\mathfrak{o}_1}_{\mathfrak{o}_S/I}) \\ V_{\mathrm{red}} (\dot{\boldsymbol{\omega}}^{\mathfrak{o}_N}_{\mathfrak{o}_N/I} - \dot{\boldsymbol{\omega}}^{\mathfrak{o}_N}_{\mathfrak{o}_E/I}) \end{bmatrix} = \\ \begin{bmatrix} \tilde{K}_{\mathfrak{o}_1} & 0_{6\times 6} \\ 0_{6\times 6} & \tilde{K}_{\mathfrak{o}_N} \end{bmatrix} \dot{e} = \begin{bmatrix} \tilde{K}_{\mathfrak{o}_1} & 0_{6\times 6} \\ 0_{6\times 6} & \tilde{K}_{\mathfrak{o}_N} \end{bmatrix} \mu, \end{aligned} \quad [36]$$

where $\tilde{K}_{\mathfrak{o}_1}, \tilde{K}_{\mathfrak{o}_N}$ are the previously diagonal gain matrices whose first and fifth rows and columns have been deleted. In conclusion, substituting the result of Eq. (36) in Eq. (33), the transformed control input $\mu \in \mathbb{R}^{12}$ is obtained

$$\mu = \begin{bmatrix} -k_{\mathfrak{o}_1} \tilde{K}^{-1}_{\mathfrak{o}_1} V_{\mathrm{red}} \boldsymbol{\omega}^{\mathfrak{o}_1}_{\mathfrak{o}_1/S} - p_{\mathfrak{o}_1} \tilde{K}^{-1}_{\mathfrak{o}_1} V_{\mathrm{red}} \left(\boldsymbol{q}^*_{\mathfrak{o}_1/S} (\boldsymbol{q}_{\mathfrak{o}_1/S} - \boldsymbol{1})^{\mathrm{S}} \right)^{\mathrm{S}} \\ -k_{\mathfrak{o}_N} \tilde{K}^{-1}_{\mathfrak{o}_N} V_{\mathrm{red}} \boldsymbol{\omega}^{\mathfrak{o}_N}_{\mathfrak{o}_N/E} - p_{\mathfrak{o}_N} \tilde{K}^{-1}_{\mathfrak{o}_N} V_{\mathrm{red}} \left(\boldsymbol{q}^*_{\mathfrak{o}_N/E} (\boldsymbol{q}_{\mathfrak{o}_N/E} - \boldsymbol{1})^{\mathrm{S}} \right)^{\mathrm{S}} \end{bmatrix}. \quad [37]$$

Incorporating μ in $\tilde{u} = E(x)^+ (\mu - \Xi(x))$, the actual values of the actuation $\tilde{u}$ are recovered.

4. Singularity Avoidance

Although, in principle, the proposed Lyapunov-based controller is able to achieve coordinated pose and velocity tracking capability, its success is subject to the full-rank condition of the matrix $E(x)$

[‡] If $\boldsymbol{a}, \boldsymbol{b}, \boldsymbol{c} \in \mathbb{H}_d$, then $\boldsymbol{a} \circ (\boldsymbol{b}\boldsymbol{c}) = (\boldsymbol{b})^{\mathrm{S}} \circ ((\boldsymbol{a})^{\mathrm{S}} \boldsymbol{c}^*) = (\boldsymbol{c})^{\mathrm{S}} \circ (\boldsymbol{b}^* (\boldsymbol{a})^{\mathrm{S}})$. See Felipe and Tsiotras.[6]

[§] Recall that a dual quaternion expressing a spatial displacement only has 6 independent elements.

introduced in Eq. (24). In fact, whenever this matrix becomes rank-deficient (i.e., $\text{rank}(E) < 12$), the problem of computing $E(x)^+$ is ill-posed. If $D = 6$ and $\text{rank}(E) < 12$, then $\det(E) = 0$ and the inverse of E does not exist; similarly, if $\text{rank}(E) < 12$ and $D > 6$, the system is inconsistent and the only possible solution is the one minimizing the error in the least-squares sense. It should be noted that $E(x)$ is a map from the the joint-space control action $\tilde{u}$ to the task-space quantity $\mu - \Xi(x)$. Therefore, whenever the manipulator is in a kinematic singular configuration, the map loses its *surjectivity* characteristics and $E(x)$ becomes rank-deficient, meaning that certain prescribed values of the end-effector acceleration are unattainable in the current configuration, no matter which force/torque is applied to the joints. In order to overcome this issue, we resort to a set-theoretic approach to the problem of singularity avoidance, exploiting the theory of Control Barrier Functions (CBF). Our aim is to ensure that our proposed Lyapunov-based solution is *forward invariant*[1] with respect to a singularity-free subset of the space of all possible solutions. This means that, if the initial robot configuration is non-singular, the CBF-constrained controller will simultaneously keep the system out of singularities and fulfil the prescribed control goal. In this way, the matrix $E(x)$ will alway maintain full-rank, and the control $\tilde{u}$ in Eq. (27) is well defined.

4.1 *Overview of Control Barrier Functions*

Consider a set $\mathcal{C}$, which we define as the superlevel set of a smooth function $h : \mathbb{R}^n \to \mathbb{R}$, that is,

$$\mathcal{C} = \{x \in \mathbb{R}^n : h(x) \geq 0\}, \tag{38}$$

and let

$$\begin{aligned} \partial\mathcal{C} &= \{x \in \mathbb{R}^n : h(x) = 0\}, \\ \text{Int}(\mathcal{C}) &= \{x \in \mathbb{R}^n : h(x) > 0\}, \end{aligned} \tag{39}$$

where $\partial\mathcal{C}$ is the *boundary* of $\mathcal{C}$ and $\text{Int}(\mathcal{C})$ its *interior*. Given an affine control system in the form described by Eq. (20), a control input $u \in \mathbb{R}^m$ renders the set $\text{Int}(\mathcal{C})$ *forward invariant* if, for every $x_0 \in \text{Int}(\mathcal{C})$, it follows that $x(t) \in \text{Int}(\mathcal{C})$ for $x(0) = x_0$ and all $t \in I(x_0)$, where $I(x_0) = [0, \tau_{\max})$ is the maximum interval of existence, such that $x(t)$ is the unique solution to Eq. (20) (see Ames et al.[1]).

Definition 1 *Let $\mathcal{C} \subset \mathbb{R}^n$ be defined by Eq. (38). Then, a function $B : Int(\mathcal{C}) \to \mathbb{R}$ is a Control Barrier Function (CBF) if there exist class $\mathcal{K}$ functions α_1, α_2[¶] and a constant $\gamma > 0$ such that, for all $x \in \mathcal{C}$,*

$$\begin{aligned} &\frac{1}{\alpha_1(h(x))} \leq B(x) \leq \frac{1}{\alpha_2(h(x))}, \\ &\inf_{u \in \mathbb{R}^m} \left[\mathcal{L}_f B(x) + \mathcal{L}_g B(x) u - \frac{\gamma}{B(x)} \right] \leq 0. \end{aligned} \tag{40}$$

Lemma 1 [**] *Given a set $\mathcal{C} \subset \mathbb{R}^n$ defined as in Eq. (38) and a continuously differentiable function $h(x) : \mathbb{R}^n \to \mathbb{R}$, if the function $B : Int(\mathcal{C}) \to \mathbb{R}$ satisfies the following conditions:*

$$\inf_{x \in \text{Int}(\mathcal{C})} B(x) \geq 0, \quad \lim_{x \to \partial\mathcal{C}} B(x) = \infty, \text{[††]} \tag{41}$$

and $B(x) \to \infty$ if and only if $x \to \partial\mathcal{C}$, then there exist class $\mathcal{K}$ functions α_1, α_2 such that

$$\frac{1}{\alpha_1(h(x))} \leq B(x) \leq \frac{1}{\alpha_1(h(x))}. \tag{42}$$

As shown in Ames et al.,[3] the existence of a CBF defined as in Eq. (40) implies the forward invariance of $\text{Int}(\mathcal{C})$. As a consequence, the set of control inputs we are interested in is expressed as

$$\begin{aligned} &K_B(x) = \\ &= \{u \in \mathbb{R}^m : \mathcal{L}_f B(x) + \mathcal{L}_g B(x) u - \frac{\gamma}{B(x)} \leq 0, \text{ for } x \in \mathcal{C}\}, \end{aligned} \tag{43}$$

where $B(x)$ can be constructed according to Eq. (41).

4.2 *Application of CBF to Singularity Avoidance*

Building upon the results reported in Section 4.1, we suggest a novel set-theoretic approach to singularity avoidance for the spacecraft robotic manipulation problem. $\text{Int}(\mathcal{C})$ introduced in Eq. (38) is identified with a singularity-free subset of the set of joint coordinates values; by achieving controlled forward invariance of $\text{Int}(\mathcal{C})$, the solution $x(t)$ of Eq. (23) will be kept away from kinematic singular configurations, hence ensuring a safe and feasible solution to the coordinated pose and velocity tracking problem. To this end, we consider a generic D-DOF manipulator characterized by F known kinematic singularities. These configurations correspond to a rank-deficient condition of the manipulator Jacobian matrix J.[14] In order to identify $\mathcal{C}$, we define F smooth

[¶] A continuous function $\alpha : [0, a) \to [0, \infty)$ is said to belong to class $\mathcal{K}$ if it is strictly increasing and $\alpha(0) = 0$. See Khalil and Hassan.[11]

[**] See Hsu et al.[9] for a proof.

[††] Note that the use of the term "barrier" comes from the fact that the value of $B(x)$ blows up on the boundary of $\mathcal{C}$.

functions $h_i(x),\ i = \{1, \cdots, F\}$, whose root(s) must correspond to value(s) of the state that cause a singular configuration. For example, if we consider a 6-revolute-joint manipulator whose configuration is the same with respect to the case study in Section 5, *elbow* and *wrist* singularities[27] arise respectively for $\Gamma_3 = 0 + k\pi, \Gamma_5 = 0 + 2k\pi,$ for $k \in \mathbb{Z}$. In this case, two valid choices of $h_1(x), h_2(x)$ are

$$\begin{aligned} h_1 &= \sin^2 \Gamma_3, \\ h_2 &= \sin^2(\Gamma_5/2); \end{aligned} \quad [44]$$

note that $h_1(0 + k\pi) = 0$ and $h_2(0 + 2k\pi) = 0$, $\forall k \in \mathbb{Z}$. In order to make the control input appear in the derivative of the control barrier function (see Eq. (43)), since the relative degree r_i of $h_i(x)$ is higher than 1 ($r_i = 2$ for constraints on the configuration), we include a first-order derivative of h_i in the construction of the CBF. Our choice is closely aligned to previous works[3,9] covering CBF-enabled constraints at the robot configuration level. Therefore, we define

$$B^i(x) = B^i_1(x) + E(\dot{h}_i(x)), \quad i \in \{1, \cdots, F\}, \quad [45]$$

where $B^i_1(x)$ has to fulfil the conditions expressed in Lemma 1 and $E(\dot{h}_i(x))$ is built according to the work of Ames et al. and Rauscher et al.[3,21] resulting in

$$B^i_1(x) = -\log\left(\frac{h_i(x)}{1+h_i(x)}\right),\ E(\dot{h}_i(x)) = a_i \frac{b_i \dot{h}_i^2(x)}{1+b_i \dot{h}_i^2(x)}, \quad [46]$$

with a_i, b_i tunable positive gains. It is straightforward to verify that the conditions described in Eq. (41) are respected. Exploiting the Lie derivatives to make the reduced input $\tilde{u}$ appear, we obtain

$$\dot{B}^i(x, \dot{x}, \tilde{u}) = \mathcal{L}_{f_i} B^i(x) + \mathcal{L}_{g_i} B^i(x)\tilde{u}, \quad [47]$$

which leads to a set of F scalar inequalities (see Eq. (43)) written in vector form,

$$A_{\text{CBF}}\tilde{u} \leq b_{\text{CBF}}, \quad [48]$$

where $A_{\text{CBF}} = \left[\mathcal{L}_{g_1} B^1(x), \cdots, \mathcal{L}_{g_F} B^F(x)\right]^T \in \mathbb{R}^{F \times (6+D)}$ and $b_{\text{CBF}} = \left[\frac{\gamma_1}{B_1(x)} - \mathcal{L}_{f_1} B^1(x), \cdots, \frac{\gamma_F}{B_F(x)} - \mathcal{L}_{f_F} B^F(x)\right]^T \in \mathbb{R}^F$. Any input $\tilde{u}$ satisfying the condition in Eq. (48) ensures that the solution to Eq. (23) stays in $\text{Int}(\mathcal{C})$, i.e. the singularity-free subset.

4.3 *Unified Tracking and Singularity Avoidance*

Previous considerations suggest that the solution to the coupled tracking and singularity avoidance problem must satisfy multiple constraints: the one related to the achievement of a desired system's performance, expressed through the DQ-CLF, and the ones enforcing singularity avoidance, written in terms of CBF. By selecting a positive definite function $W(x) = k_{\mathfrak{o}_1}(\boldsymbol{\omega}^{\mathfrak{o}_1}_{\mathfrak{o}_1/S})^{\text{S}} \circ (\boldsymbol{\omega}^{\mathfrak{o}_1}_{\mathfrak{o}_1/S})^{\text{S}} + k_{\mathfrak{o}_N}(\boldsymbol{\omega}^{\mathfrak{o}_N}_{\mathfrak{o}_N/E})^{\text{S}} \circ (\boldsymbol{\omega}^{\mathfrak{o}_N}_{\mathfrak{o}_N/E})^{\text{S}}$ (see Eq. (29)), the constraint $\dot{V}(x) \leq -W(x)$ can be rearranged using Lie derivatives, becoming

$$\psi_0(x) + \psi_1^T(x)\tilde{u} \leq 0, \quad [49]$$

with $\psi_0(x) = \mathcal{L}_f V(x) + W(x)$ and $\psi_1(x) = \mathcal{L}_g V(x)^T \in \mathbb{R}^{6+D}$. The DQ-CLF and CBF constraints can then be unified through a quadratic program (QP).[1–3,9,21] This results in a DQ-CLF-CBF-QP in the form

$$\begin{aligned} u^*(x) = \underset{\boldsymbol{u}=\begin{bmatrix}\tilde{u}\\ \delta\end{bmatrix} \in \mathbb{R}^{6+D+1}}{\arg\min} \quad & \frac{1}{2}\boldsymbol{u}^T H(x)\boldsymbol{u} + F^T(x)\boldsymbol{u} \\ \text{s.t.} \quad & \psi_0(x) + \psi_1^T(x)\tilde{u} \leq \delta, \\ & \mathcal{L}_{f_1} B^1(x) + \mathcal{L}_{g_1} B^1(x)\tilde{u} \leq \frac{\gamma_1}{B_1(x)}, \\ & \vdots \\ & \mathcal{L}_{f_F} B^F(x) + \mathcal{L}_{g_F} B^F(x)\tilde{u} \leq \frac{\gamma_F}{B_F(x)}, \end{aligned} \quad [50]$$

where the scalar δ guarantees the existence of a solution to Eq. (50) by relaxing the condition dictated by the CLF. This means that whenever the conditions expressed by the CLF and the CBF are in conflict, the system will enforce respect of the constraints expressed by the CBF, while temporarily losing sight of the control objective. When instead the two conditions do not conflict, they will be achieved simultaneously. In their turn, $H(x)$ and $F(x)$ can be obtained upon definition of the quadratic cost function $\mathcal{J}(\boldsymbol{u})$ to be minimized by the QP. In a compact form, introducing

$$A = \begin{bmatrix} \psi_1^T & -1 \\ A_{\text{CBF}} & 0_{F\times 1} \end{bmatrix} \in \mathbb{R}^{(1+F)\ \times\ (6+D+1)} \quad [51]$$

and

$$b = \begin{bmatrix} -\psi_0 \\ b_{\text{CBF}} \end{bmatrix} \in \mathbb{R}^{1+F}, \quad [52]$$

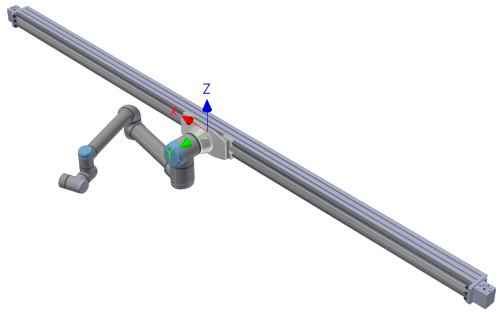

Fig. 4: CAD model of the UR10e manipulator. The system features a collaborative 6-DOF manipulator mounted on a cart free to translate along the x-axis.

Eq. (50) becomes

$$u^*(x) = \underset{\boldsymbol{u}=\begin{bmatrix}\tilde{u}\\ \delta\end{bmatrix}\in\mathbb{R}^{6+D+1}}{\arg\min} \quad \frac{1}{2}\boldsymbol{u}^T H \boldsymbol{u} + F^T \boldsymbol{u} \qquad \text{s.t.} \quad A\boldsymbol{u} \leq b, \tag{53}$$

which can be readily solved using one of the many existing QP algorithms.

5. Results

The ideas displayed so far can be specialized to describe any kind of joint spacecraft-manipulator architecture, provided that it can be modeled in a graph-like way as shown in Fig. 1. Without losing generality, but instead proving the flexibility of the proposed formulation, we specialize the general framework to the case illustrated in Fig. 4, consisting in a 6-DOF UR10e collaborative robot free to translate along a rail; the robot is modeled as the manipulator, while the sliding base is dealt with using the satellite-base equations. Although characterized by a single translational degree of freedom of the base, assuming no external forces, the kinematic and dynamic interactions between this system's components are the same described in Sections 2.3 and 2.4. The quantities characterizing the system's topology (see Section 2.3) are defined in Table 2. The end-effector frame is coincident with the last body frame ($\mathcal{F}_7$), hence no additional coordinate system has been introduced in order to describe the tracking maneuver.

Param.	Desc.	Quantity
N	Bodies	7
J	Joints	6
D	DOF allowed	6
R	DOF constrained	30

Table 2: Topology of a 6R spacecraft-mounted manipulator.

5.1 *DQ Reference Generation*

The reference base (S) and end-effector (E) trajectories evolve as follows:

$$\begin{aligned} x_S &= x^I_{\mathfrak{o}_1/I} + \Delta x \\ y_S &= 0 \\ z_S &= 0 \end{aligned} \qquad \begin{aligned} x_E(t) &= r_{0,x} + r\cos(\omega_r t) \\ y_E(t) &= r_{0,y} + r\sin(\omega_r t) \\ z_E &= r_{0,z} \\ \phi_E(t) &= \Phi\sin(\omega_\phi t) \end{aligned}$$

with

$$\begin{aligned} r_{0,x} &= 0.5[m],\ \omega_r = 0.2[rad/s] \\ r_{0,y} &= 1[m],\ r_{0,z} = -0.08[m] \\ \Phi &= \pi/3[rad],\ \omega_\phi = 0.5[rad/s] \end{aligned}$$

where the base only has one degree of freedom because of the rail constraint.

While the end-effector tracks a circular trajectory in the XY-plane described by $\bar{r}^I_{E/I} = \left[x_E(t), y_E(t), z_E\right]$, along with a time varying attitude described by the yaw angle $\phi_E(t)$, the base is used to bring the manipulator in an optimal position to perform the tracking maneuver, as an example of a *coordinated control* strategy. Such a position corresponds to a predefined *offset* distance between the robot anchor point and a characteristic point of the trajectory to be tracked, which in the case under analysis is the center of the circle, r_0. This offset is needed to avoid occurrence of the so-called *shoulder* singularity, which takes place whenever the intersection of the fifth and sixth axes lies in the plane defined by the axes of the first and second joints.[27] Hence, by defining the value of the offset as $\lambda/2$, Δx is the error between the current position of the base along the rail and its target position, and the following relationship holds

$$\left\| x^I_{\mathfrak{o}_1/I} - r_{0,x} \right\| = \|\Delta x\| + \frac{\lambda}{2}. \tag{54}$$

5.2 *Numerical Results*

The system presented has been simulated in a joint MATLAB/SIMULINK environment to the aim

Control Lyapunov Function parameters	
Base	End-effector
$\tilde{K}_{\mathfrak{o}_1} = I_6, k_{\mathfrak{o}_1} = 3, p_{\mathfrak{o}_1} = 3$	$\tilde{K}_{\mathfrak{o}_N} = I_6, k_{\mathfrak{o}_N} = 1, p_{\mathfrak{o}_N} = 1$
Control Barrier Functions parameters	
Elbow	Wrist
$a_E = 1, b_E = 1, \gamma_E = 1$	$a_W = 150, b_W = 50, \gamma_W = 10$

Table 3: Parameters for the coordinated DQ-CLF-CBF-QP controller.

Initial Conditions		
Base Pose	Joints Coord.	Dual vel.
$\boldsymbol{q}_{\mathfrak{o}_1/I} = \boldsymbol{1}$	$\Gamma_{J_1,0} = 90^\circ$	$\boldsymbol{\omega}^{\mathfrak{o}_1}_{\mathfrak{o}_1/I,0} = \boldsymbol{0}$
-	$\Gamma_{J_2,0} = 100^\circ$	$\boldsymbol{\omega}^{\mathfrak{o}_2}_{\mathfrak{o}_2/I,0} = \boldsymbol{0}$
-	$\Gamma_{J_3,0} = 120^\circ$	$\boldsymbol{\omega}^{\mathfrak{o}_3}_{\mathfrak{o}_3/I,0} = \boldsymbol{0}$
-	$\Gamma_{J_4,0} = 0^\circ$	$\boldsymbol{\omega}^{\mathfrak{o}_4}_{\mathfrak{o}_4/I,0} = \boldsymbol{0}$
-	$\Gamma_{J_5,0} = 90^\circ$	$\boldsymbol{\omega}^{\mathfrak{o}_5}_{\mathfrak{o}_5/I,0} = \boldsymbol{0}$
-	$\Gamma_{J_6,0} = 0^\circ$	$\boldsymbol{\omega}^{\mathfrak{o}_6}_{\mathfrak{o}_6/I,0} = \boldsymbol{0}$
-	-	$\boldsymbol{\omega}^{\mathfrak{o}_7}_{\mathfrak{o}_7/I,0} = \boldsymbol{0}$

Table 4: Initial conditions for the simulation.

of proving tracking capability with respect to the base and end-effector trajectories, while also ensuring avoidance of kinematic singularities. The parameters defining the controller and the initial conditions of the simulation are reported respectively in Table 3 and Table 4. The initial values of the joint coordinates $\Gamma_{J_i,0}$ correspond to a folded configuration of the arm and were chosen to start the simulation in a *high-manipulability* [‡‡] condition. Fig. 5 displays convergence of the pose DQ errors of the base, while Fig. 6 shows the same quantities referred to the end-effector. A physical interpretation of the positioning performance is enabled by Fig. 7, which reports the comparison between the current and target position of the end-effector. As shown in Fig. 7, the circular reference to be followed by the end-effector is initially out of the reachable region of the manipulator; however, in accordance with the coordinated control philosophy, the tracking maneuver is still feasible thanks to the suitable motion of the base.

[‡‡]The *manipulability* is defined as the ability of a robotic mechanism to position and orient its end-effector. Different measures of manipulability have been proposed; to the aim of this study, we use the *manipulability index* $w = \sqrt{\det(JJ^T)}$[31]. The lower w, the lower the manipulability.

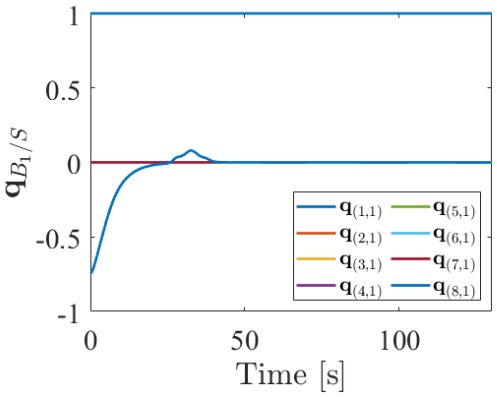

Fig. 5: DQ error between current (B_1) and desired (S) pose of the base.

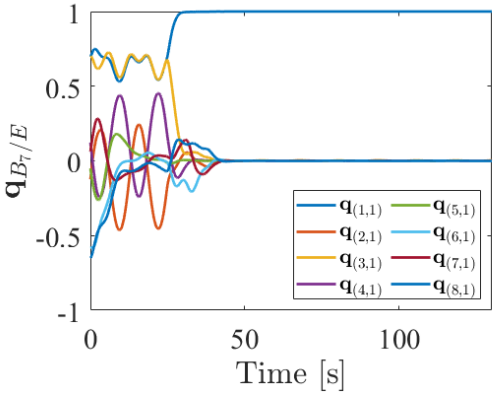

Fig. 6: DQ error between current (B_7) and desired (E) pose of the end-effector.

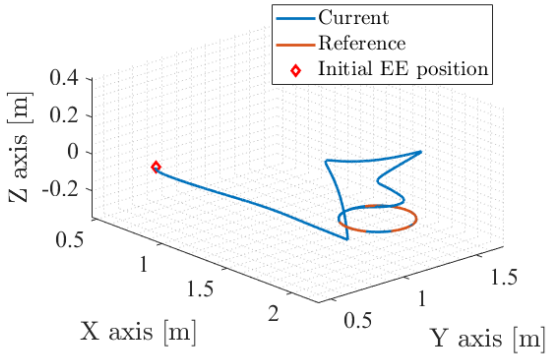

Fig. 7: Tracking result of the trajectory. The straight blue line corresponds to the end-effector motion caused by the base in order to bring the manipulator close to its optimal maneuvering position.

In addition to the coordinated pose-tracking capability, the proposed controller is also able to avoid kinematic singularities that may be encountered while driving the system towards the desired configuration.

Singularity avoidance through Control Barrier Function (CBF) has been assessed comparing our strategy, consisting in the solution of the DQ-CLF-CBF-QP in Eq. (50), to the nominal solution to the pose-tracking problem, without any additional constraint enforcing singularity avoidance. In this case, the reduced control input $\tilde{u}$ is computed through direct inversion of the linear system in Eq. (27).

The two approaches have been compared in terms of value of the manipulability index w, accuracy of the solution and smoothness of the computed control torque profile. The direct solution of Eq. (27) results in multiple spikes in the control action profile due to numerical issues in correspondence of a close-to-singular condition. The desired tracking accuracy is however obtained when the robot is in a high-manipulability state. The proposed DQ-CLF-CBF-QP is able to both preserve a nonzero value of the manipulability index and a smooth actuation profile. In addition, after steering the end-effector away from a singular condition, it retrieves the same accuracy of the nominal solution.

6. Conclusion

This paper exploited the dual quaternion (DQ) framework to provide a description of the kinematics and dynamics of a spacecraft-mounted manipulator. By leveraging the compact DQ formulation of spatial rigid body motions, a dual quaternion Control Lyapunov Function (DQ-CLF) has been designed to achieve coordinated tracking of a time-varying pose with both the satellite-base and the end-effector. In order to ensure feasibility and robustness of the proposed solution, we envisioned a Control Barrier Function (CBF) based singularity avoidance method which has been integrated with the DQ-CLF in the context of a quadratic program (QP). As proved by the results of numerical simulations, the solution of the resulting DQ-CLF-CBF-QP displayed both *performance* and *safety* in terms of reference tracking and kinematic singularity avoidance.

References

[1] A. D. Ames, S. Coogan, M. Egerstedt, G. Notomista, K. Sreenath, and P. Tabuada. Control barrier functions: Theory and applications. In *2019 18th European Control Conference*, pages 3420–3431. IEEE, 2019.

[2] A. D. Ames, J. W. Grizzle, and P. Tabuada. Control barrier function based quadratic programs with application to adaptive cruise control. In *53rd IEEE Conference on Decision and Control*, pages 6271–6278. IEEE, 2014.

[3] A. D. Ames, X. Xu, J. W. Grizzle, and P. Tabuada. Control barrier function based quadratic programs for safety critical systems. *IEEE Transactions on Automatic Control*, 62, 2017.

[4] A. Antonello, A. Valverde, and P. Tsiotras. Dynamics and control of spacecraft manipulators with thrusters and momentum exchange devices. *Journal of Guidance, Control, and Dynamics*, 42, 2019.

[5] F. Caccavale and B. Siciliano. Quaternion-based kinematic control of redundant spacecraft/manipulator systems. In *Proceedings 2001 ICRA. IEEE International Conference on Robotics and Automation*, volume 1, pages 435–440. IEEE, 2001.

[6] N. Filipe and P. Tsiotras. Rigid body motion tracking without linear and angular velocity feedback using dual quaternions. In *2013 European Control Conference*, pages 329–334. IEEE, 2013.

[7] N. Filipe and P. Tsiotras. Simultaneous position and attitude control without linear and angular velocity feedback using dual quaternions. In *2013 American Control Conference*, pages 4808–4813. IEEE, 2013.

[8] A. Flores-Abad, O. Ma, K. Pham, and S. Ulrich. A review of space robotics technologies for on-orbit servicing. *Progress in Aerospace Sciences*, 68:1–26, 2014.

[9] S. Hsu, X. Xu, and A. D. Ames. Control barrier function based quadratic programs with application to bipedal robotic walking. In *2015 American Control Conference*, pages 4542–4548. IEEE, 2015.

[10] H. S. Jayakody, L. Shi, J. Katupitiya, and N. Kinkaid. Robust adaptive coordination controller for a spacecraft equipped with a robotic manipulator. *Journal of Guidance, Control, and Dynamics*, 39:2699–2711, 2016.

[11] H. K. Khalil. *Nonlinear Systems*, chapter 13. Prentice-Hall, Upper Saddle River, NJ, 3 edition, 2002.

[12] B. Liang, Y. Xu, and M. Bergerman. Dynamically equivalent manipulator for space manipulator system. 1. In *Proceedings of International Conference on Robotics and Automation*, volume 4, pages 2765–2770. IEEE, 1997.

[13] B. Liang, Y. Xu, M. Bergerman, and G. Li. Dynamically equivalent manipulator for space manipulator system. 2. In *Proceedings of the 1997 IEEE/RSJ International Conference on Intelligent Robot and Systems. Innovative Robotics for Real-World Applications. IROS '97*, volume 3, pages 1493–1499. IEEE, 1997.

[14] K. M. Lynch and F. C. Park. *Modern Robotics: Mechanics, Planning, and Control*, chapter 5, pages 191–199. Cambridge University Press, New York, NY, United States, 1 edition, 2017.

[15] Y. Nakamura and R. Mukherjee. Nonholonomic path planning of space robots. In *Proceedings, 1989 International Conference on Robotics and Automation*, volume 2, pages 1050–1055. IEEE, 1989.

[16] NASA. On-Orbit Satellite Servicing Study, Project Report. 2010.

[17] M. Oda. Coordinated control of spacecraft attitude and its manipulator. In *Proceedings of IEEE International Conference on Robotics and Automation*, volume 1, pages 732–738. IEEE, 1996.

[18] E. Papadopoulos and S. Dubowsky. Coordinated manipulator/spacecraft motion control for space robotic systems. In *Proceedings. 1991 IEEE International Conference on Robotics and Automation*, volume 2, pages 1696–1701. IEEE, 1991.

[19] E. Papadopoulos and S. Dubowsky. The kinematics, dynamics, and control of free-flying and free-floating space robotic systems. *IEEE Transactions on Robotics and Automation*, 9:531–543, 1993.

[20] O. Parlaktuna and M. Ozkan. Adaptive control of free-floating space manipulators using dynamically equivalent manipulator model. *Robotics and Autonomous Systems*, 46:185–193, 2004.

[21] M. Rauscher, M. Kimmel, and S. Hirche. Constrained robot control using control barrier functions. In *2016 IEEE/RSJ International Conference on Intelligent Robots and Systems*, pages 279–285. IEEE, 2016.

[22] Y. Umetani and K. Yoshida. Continuous path control of space manipulators mounted on omv. *Acta Astronautica*, 15, 1987.

[23] Z. Vafa and S. Dubowsky. On the dynamics of manipulators in space using the virtual manipulator approach. In *Proceedings. 1987 IEEE International Conference on Robotics and Automation*, volume 4, pages 579–585. IEEE, 1987.

[24] A. Valverde and P. Tsiotras. Dual quaternion framework for modeling of spacecraft-mounted multibody robotic systems. *Frontiers in Robotics and AI*, 5:128, 2018.

[25] A. Valverde and P. Tsiotras. Spacecraft robot kinematics using dual quaternions. *Robotics*, 7, 2018.

[26] A. Valverde and P. Tsiotras. Dual quaternions as a tool for modeling, control, and estimation for spacecraft robotic servicing missions. *The Journal of the Astronautical Sciences*, 67:595—-629, 2020.

[27] M. Weyrer, M. Brandstötter, and M. Husty. Singularity avoidance control of a non-holonomic mobile manipulator for intuitive hand guidance. *Robotics*, 8, 2019.

[28] M. Wilde, J. Harder, and E. Stoll. Editorial: On-orbit servicing and active debris removal: Enabling a paradigm shift in spaceflight. *Frontiers in Robotics and AI*, 6, 2019.

[29] Y. Yang. Spacecraft attitude determination and control: Quaternion based method. *Annual Reviews in Control*, 36, 2012.

[30] K. Yoshida and H. Nakanishi. Impedance matching in capturing a satellite by a space robot. In *Proceedings 2003 IEEE/RSJ International Conference on Intelligent Robots and Systems*, volume 3, pages 3059–3064. IEEE, 2003.

[31] T. Yoshikawa. Manipulability of robotic mechanisms. *The International Journal of Robotics Research*, 4, 1985.